AJNR Am J Neuroradiol 20:237–245, February 1999

In Vitro and In Vivo Comparison of Three MR Measurement Methods for Calculating Vascular Shear Stress in the Internal Carotid Artery

Anthony M. Masaryk, Richard Frayne, Orhan Unal, Elizabeth Krupinski, and Charles M. Strother

BACKGROUND AND PURPOSE: **Vascular abnormalities, such as atherosclerosis and the growth and rupture of cerebral aneurysms, result from a derangement in tissue metabolism and injury that are, in part, regulated by hemodynamic stress. The purpose of this study was to establish the feasibility and accuracy of determining wall shear rate in the internal carotid artery from phase-contrast MR data.**

METHODS: **Three algorithms were used to generate shear rate estimates from both ungated and cardiac-gated 2D phase-contrast data. These algorithms were linear extrapolation (LE), linear estimation with correction for wall position (LE*), and quadratic extrapolation (QE). In vitro experiments were conducted by using a phantom under conditions of both nonpulsatile and pulsatile flow. The findings from five healthy volunteers were also studied. MR imaging–derived shear rates were compared with values calculated by solving the fluid flow equations.**

RESULTS: **Findings of in vitro constant-flow experiments indicated that at one or two excitations, QE has the advantage of good accuracy and low variance. Results of in vitro pulsatile flow experiments showed that neither LE* nor QE differed significantly from the predicted value of wall shear stress, despite errors of 17% and 22%, respectively. In vivo data showed that QE did not differ significantly from the predicted value, whereas LE and LE* did. The percentages of errors for QE, LE, and LE* in vivo measurements were 98.5%, 28.5%, and 36.1%, respectively. The average residual of QE was low because the residuals were both above and below baseline whereas, on average, LE* tended to be a more biased overestimator of the shear rate in volunteers. The average and peak wall shear force in five volunteers was approximately 8.10 dyne/cm^2 and 13.2 dyne/cm^2, respectively.**

CONCLUSION: **Our findings show that LE consistently underestimates the shear rate. Although LE* and QE may be used to estimate shear rate, errors of up to 36% should be expected because of variance above and below the true value for individual measurements.**

Vascular disease occurs as a result of a derangement in cellular metabolism of the vascular wall and the inability of the vasculature to withstand the force that the flowing blood exerts on it. Cellular metabolism and morphologic features appear to be regulated in part by the mechanical forces exerted by the flow of blood (1–4). In addition, the patterns of flow near a vessel wall may determine how much interaction there is between the wall and blood-borne cellular elements (1). A complete description of the hemodynamics within a particular vessel or lesion requires knowledge of the geometry and mechanical properties of the vascular wall, the pressure, the viscosity and density of blood, and the pattern of blood velocities within the stream of flow (5–7). Knowledge of the pattern of velocity near the vessel wall and the force exerted on it may provide quantitative parameters for estimating the risk of progression of atherosclerosis, growth and rupture of cerebral aneurysms, and venous hypertension and hemorrhage associated with arteriovenous malformations (8–14). MR imaging and phase-contrast (PC) velocity measurements potentially provide vascular geometry and detailed measurement of blood flow velocities (15–17). With

Received April 21, 1998; accepted after revision November 2.

Supported by a Berlex/ASNR Fellowship (A.M.M.) and by the Heart and Stroke Foundation of Canada (R.F.).

Presented in part at the annual meeting of the American Society of Neuroradiology, Seattle, June 1996.

From the Departments of Radiology (R.F., O.U., C.M.S.) and Medical Physics (R.F., O.U.), Clinical Science Center, University of Wisconsin-Madison; and the Department of Radiology, University of Arizona Health Sciences Center, Tucson (A.M.M., E.K.).

Address reprint requests to Anthony M. Masaryk, MD, Department of Radiology, University of Arizona Health Sciences Center, P.O. Box 245067, 1501 N Campbell Ave, Tucson, AZ 85724.

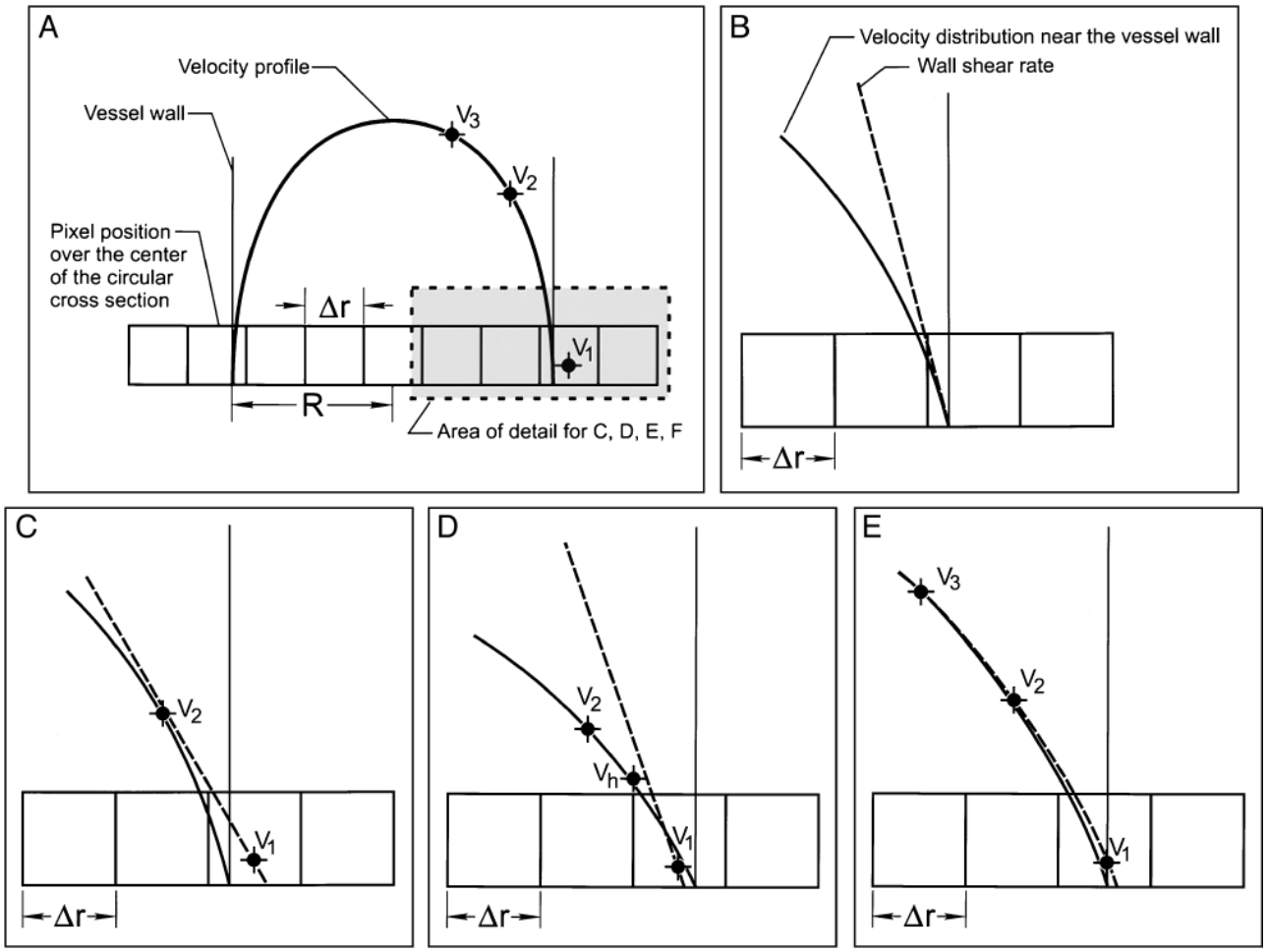

FIG 1. Velocity distribution and shear rate at the vessel wall.

A, View of the velocity profile along the horizontal row of shaded pixels. Note that the boundary between the vessel lumen and the vessel wall will not coincide with a pixel edge; thus, in general, edge pixels will contain signals from flowing fluid and the stationary vessel wall.

B–E, Detail near the vessel wall showing the actual velocity gradient. Calculation of wall shear rate using LE (*C*), LE* (*D*), and QE (*E*). Velocity measurements in the edge pixels and the two adjacent pixels are denoted by v_1, v_2, and v_3, respectively.

these data in hand, only reasonable assumptions of blood density and viscosity are needed to be able to calculate the forces acting on the vessel wall (7). Previous studies have used MR imaging to measure pulsatile pressure gradients (18). In this feasibility study, we calculated another term in the equation describing the balance of hemodynamic force at the vascular wall; that is, shear stress. Shear stress is the drag on the vessel wall caused by the flow of blood down its length, and it has been implicated by a number of researchers as being an important physiological parameter for both the initiation and the promotion of vascular disease (1–3, 7–11). Because of the potential significance of shear stress, a number of other groups have used PC MR velocity data to measure it, primarily within large-caliber vessels such as the aorta (19–21).

Shear rate (γ) is the gradient or slope of the axial velocity (v) profile with respect to radial position (r), as shown in Figure 1A:

$$\gamma = \frac{\partial v}{\partial r}, \quad (1)$$

Shear stress (τ_w), the drag force exerted by the flowing blood on the vessel wall, is equal to the product of the shear rate at the wall and the viscosity of blood (μ) (7):

$$\tau_w = \mu\gamma = \mu\frac{\partial v}{\partial r}. \quad (2)$$

The purpose of this study was to investigate the accuracy and establish the feasibility of three different methods for calculating shear rate from PC MR data: linear extrapolation (LE), linear estimation with correction for wall position (LE*), and quadratic extrapolation (QE) (19, 22, 23). All three algorithms approximate the slope of the velocity

profile with respect to position along the radius of the vessel at a particular point; that is, the vessel wall (where velocity should be zero). Linear extrapolation, as the name implies, approximates the slope of the curve by assuming that it is a line. The two measured velocities near the wall are used to calculate the slope of the line assumed to pass through them. Similarly, QE consists of fitting a quadratic (containing a squared variable, in this case, radial position [r^2]) or a parabolic curve to three points and then calculating the slope of this curve at the wall.

The feasibility of using the methods described was investigated by means of a series of experiments of progressively increasing complexity. The first, and simplest, experiment was the measurement of shear rate in nonpulsatile, laminar flow in a circular cylindrical phantom. Wall shear rate was then measured in the same phantom by using pulsatile flow and a physiological carotid artery flow waveform that was generated by using a computer-controlled flow simulator. Finally, the same analysis schemes were performed on PC data obtained from the cervical segment of the internal carotid artery of five healthy volunteers. The accuracy and precision of the measurements were analyzed.

Methods

MR Measurements and Shear Derivations

How PC velocity measurements in pixels at and adjacent to the vessel wall may be used to approximate the velocity gradient at the vessel wall is shown in Figure 1B--E, where v_1 is the velocity measured at the wall and v_2 and v_3 are the velocities measured in the adjacent pixels in the vessel (19, 22, 23). Determination of the velocity gradient from PC velocity estimates obtained at discrete locations (ie, pixels), however, introduces two sources of systematic errors. First, in regions where the velocity gradients are large, the PC measurements generally overestimate the true mean velocity within the pixel because of the nonlinear effects of intravoxel dephasing and blood saturation (24). This effect can be minimized by using small pixels. Second, velocity estimates from pixels that contain both vessel wall and flowing blood may be erroneous because of the differences in signal intensity and saturation between blood and wall tissue (25). This partial-volume effect error can be corrected by estimating the position of the vessel wall within the pixel that contains the interface between the vessel lumen and the wall. The LE* and QE algorithms attempt this correction, whereas the LE does not (19, 22, 23).

To approximate the wall shear rate, the LE method of assessment (Fig 1C) requires two velocity measurements, one obtained at, and the other near, the wall (v_1, v_2, respectively) (23)

$$\gamma = \frac{v_2 - v_1}{\Delta r}. \quad (3)$$

An improved LE technique (LE*), developed by Oshinski et al (19), allows estimation of the vessel wall position within the pixel at the wall (Fig 1D). This wall position estimate (x, where $0 < x < \Delta r$) is determined by first estimating the velocity value at the pixel edge, v_h, by averaging the velocity of the pixel at the wall and the adjacent pixel containing only flowing blood:

$$v_h = \frac{v_2 + v_1}{2}. \quad (4)$$

By invoking the conservation of mass, the fraction of the edge pixel occupied by flowing blood may be shown to be

$$x = \frac{2v_1\Delta r}{v_h}. \quad (5)$$

Assuming a linear velocity profile across the voxel containing the wall, an estimate for the velocity gradient at the wall after correcting for wall position is

$$\gamma = \frac{v_h}{x} = \frac{v_h^2}{2v_1\Delta r}. \quad (6a)$$

Additional adjustments to this expression were found to be necessary, primarily to account for the effect of noise on x, particularly when x is less than 0.2 or greater than 1.0. For $x < 0.2$,

$$\gamma = \frac{v_2}{\frac{\Delta r}{2} + x}, \quad (6b)$$

and for $x > 1.0$,

$$\gamma = \frac{v_2}{\Delta r}. \quad (6c)$$

For QE (Fig 1E), the velocity gradient near the wall is assumed to be parabolic (5):

$$v = ar^2 + br + c. \quad (7)$$

where a, b, and c are unknown constants. The shear rate at the wall is,

$$\gamma = \left.\frac{dv}{dr}\right|_{r = R} = 2aR + bR, \quad (8)$$

where a and b may be derived algebraically using three velocity measurements (v_1, v_2, v_3) obtained from the three pixels at and adjacent to the vessel wall (23) (R = maximal tube or vessel diameter).

Flow Apparatus

The experimental flow phantom consisted of a straight, cylindrical agar tube (radius $R = 0.32$ cm) surrounded by a solid block of agar (26). The phantom was specifically designed to ensure that no signal void is found at the interface between the tissue-mimicking material and the blood-mimicking fluid (ie, lumen wall interface). An absence of signal from the vessel wall, such as would occur in an acrylic or glass phantom, would cause unrealistic signals at the vessel-wall lumen interface and would thus confound assessment of shear rate measurements (21). A computer-controlled flow simulator (Shelley Medical Imaging Technologies, London, Ontario, Canada) was used to generate both nonpulsatile and pulsatile flow waveforms. Constant flow was generated at a rate of 5 mL/s, with an accuracy and precision of ±1%. A previously described physiological carotid waveform was also generated in the flow phantom, with an average flow rate of 1.7 mL/s (5.5 cm/s) and a peak systolic flow rate of 9.9 mL/s (32 cm/s) (27). A blood-mimicking fluid with density (1.0 g/cm^3) and viscosity (2.9 cP ± 0.1 cP) similar to human blood was used in the apparatus. The MR relaxation rates of the tissue- and blood-mimicking materials are similar to conditions expected in vivo (27, 28). An ultrasonic transit-time probe (Transonics Systems, Ithaca, NY) was used to monitor the pulsatile flow waveforms.

Pulse Sequences

A cardiac-gated 2D PC pulse sequence was used to measure the axial component of flow velocity in the phantom and in the human subjects. All MR velocity data were acquired using a 2D PC technique on a 1.5-T MR unit, with imaging parameters of 40/3 (TR/TE), a flip angle of 25°, a 10-mm-thick slab oriented perpendicular to the vessel of interest, and a 256 × 192 acquisition matrix. The velocity-encoding value was 100 cm/s, and the reconstructed pixel dimensions were 0.7 mm × 0.7 mm × 10.0 mm. Measurements of pulsatile flow acquisitions were acquired using retrospective gating, so that 16 phases per cardiac cycle were reconstructed. To examine the effect of signal-to-noise ratio on the accuracy and precision of the shear rate estimates, a series of constant-flow experiments was repeated using different numbers of signal averages (sequences with one, two, four, eight, and 16 acquisitions). All other sequences had one acquisition. The same pulse sequence was used to scan the cervical segment of the internal carotid artery in five healthy volunteers. All human studies were conducted with a protocol approved by the institutional review board, and written informed consent was obtained from all volunteers before the study.

Calculated Wall Shear Rate Estimates

Wall shear rate estimates were calculated from the Navier-Stokes equations by using the volume flow rates and by applying suitable boundary conditions and simplifying assumptions. These assumptions included the following: that flow is laminar, that the fluid is Newtonian, and that the vessel is infinitely long and circular. The calculated shear rates were used as the standard against which the LE, LE*, and QE shear rate estimates were compared. A similar procedure has been used previously to assess the accuracy of velocity profiles in pulsatile flow obtained with PC MR imaging (28). For nonpulsatile flow in a straight circular tube, the wall shear rate can be related to the average velocity, $\bar{v}$, if the fluid viscosity and density are known (7). For the constant laminar flow, the velocity distribution in a straight tube is parabolic,

$$v(r) = 2\bar{v}\left(1 - \left(\frac{r}{R}\right)^2\right). \quad 9)$$

The shear rate at the tube wall is, therefore, given by

$$\gamma = \frac{dv}{dr} = -\frac{4\bar{v}}{R}. \quad 10)$$

For pulsatile flow, the Womersley formulation of the Navier-Stokes equation must be used to numerically determine shear rate, again assuming that the vessel walls are rigid (29, 30). Given a time series of average velocities, $\bar{v}(t)$, the time-varying shear rate at the wall can then be calculated using the procedure described by Frayne et al (28). The time series of average velocities was obtained using both PC MR data and, for some of the in vitro experiments, an ultrasonic flow probe. Briefly, this procedure consisted of expressing $\bar{v}(t)$ as a Fourier series,

$$\bar{v}(t) = \sum_k V_k \cos(k\omega_o + \theta_k), \quad 11)$$

where V_k and $(\theta)_k$ are the Fourier coefficient and phase of the k-th harmonic, and ω_o is the fundamental frequency. The velocity profile, $v_k(r,t)$, for each harmonic $[V_k \cos(k\omega_o + \theta_k)]$ is found by using Womersley's solution to the Navier-Stokes equation. All velocity profiles are summed to obtain the overall velocity profile for the $\bar{v}(t)$ flow waveform,

$$v(r, t) = \sum_k v_k(r, t). \quad 12)$$

The derivative of this expression is then obtained and evaluated at the wall ($r = R$) to determine the wall shear rate.

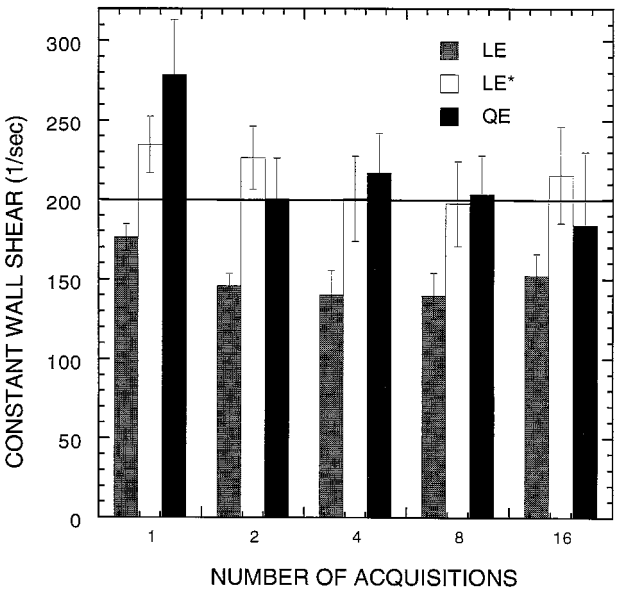

FIG 2. Measured shear rates for a constant-flow experiment in the phantom. The predicted shear rate at the wall was 198 s^{-1}. Experiments were repeated using different numbers of signal averages (*NEX*). Error bars represent ±1 SE.

Data Analysis

To aid in the analysis of PC MR velocity data, a software tool was developed on a workstation (Sparc 10; Sun Microsystems, Sunnyvale, CA). The tool consisted of two components: the first part allowed pixels at the vessel wall to be identified, and the second part calculated the shear rate at these locations. In initial experiments, vessel edge detection was optimized by first displaying the complex differences of the MR data acquired with opposite flow encodings for a series of pixels traversing the vessel. Later, this step was abandoned, and edge detection was accomplished by having the operator move the cursor over the magnitude image and manually identify the edge pixels. With suitable operator training, both approaches yielded the same results.

Shear rate was calculated near four edge pixels located at the four cardinal positions around the circumference of the vessel (denoted left, top, right, and bottom). The tool allowed shear rates to be estimated using velocities obtained from the pixel at the wall as well as from either one (LE and LE*) or two (QE) adjacent pixels within the vessel. Because of the circular symmetry of both the phantom and the cervical segment of the internal carotid artery, the shear rate measurement was averaged over the four measurements obtained around the circumference of the vessel. This process was repeated for data sets obtained for each cardiac phase, both in the pulsatile flow phantom experiments and in the human studies.

Statistical analysis of the constant-flow wall shear rate measurements was performed using a repeated measures analysis of variance test. Post-hoc analysis (Fisher protected least squares difference) on the overall number of acquisitions was also performed. The statistical significance of differences between the three algorithms and the calculated shear rates in the volunteers was accomplished using a post-hoc analysis (31).

Results

In Vitro Experiments

The results of the in vitro constant-flow experiments are shown in Figure 2 for different numbers of signal averages. The accuracy of the measured shear rates calculated with all three methods tended

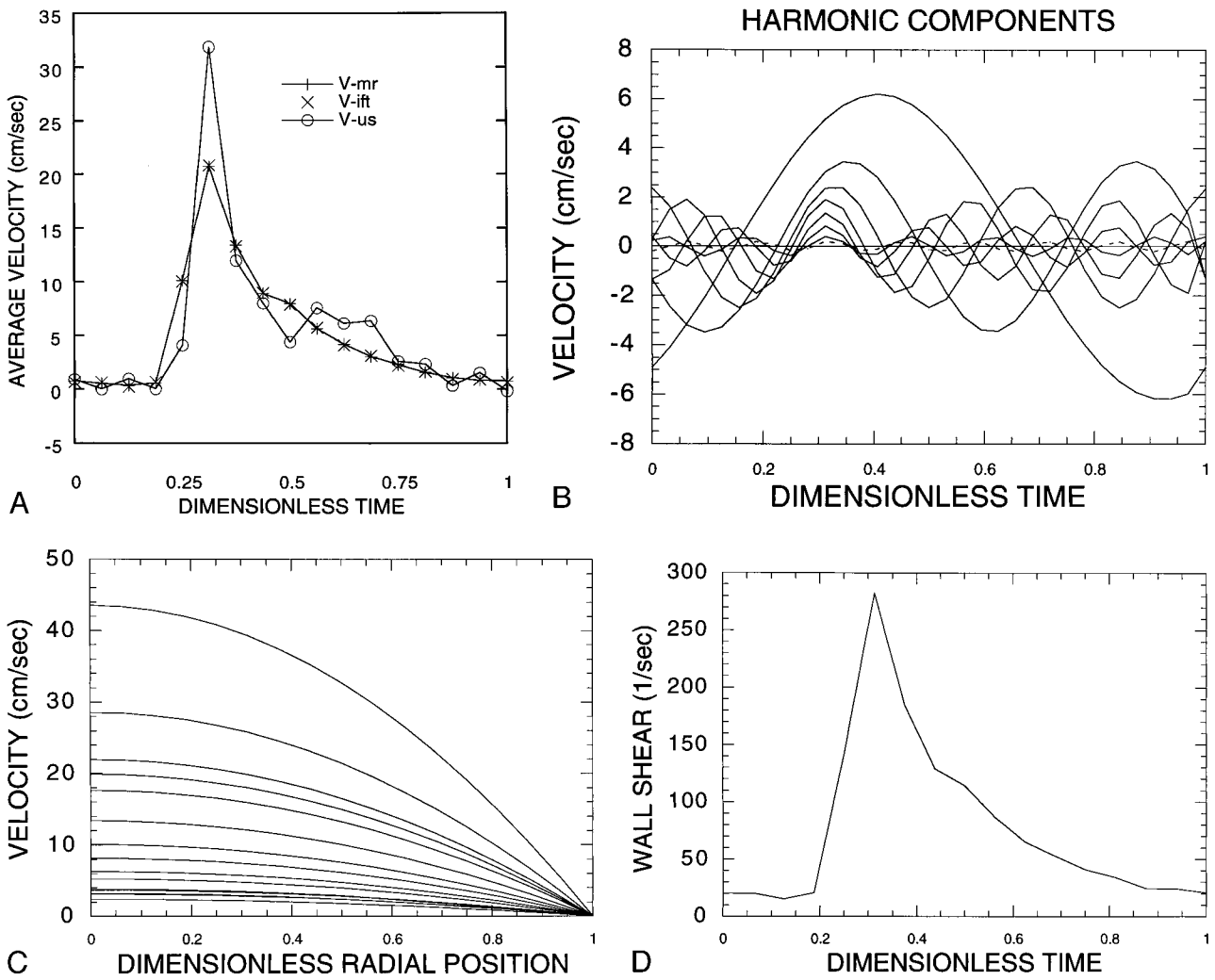

FIG 3. Measured shear rates for the pulsatile flow experiment in the phantom.

A, Pulsatile average velocity waveform measured by retrospectively gated 2D PC MR imaging (*V-mr*), reconstructed from a Fourier decomposition of harmonic components (*V-ift*) and independently measured using an ultrasonic flow probe (*V-us*).

B, Fourier harmonic components of the pulsatile average velocity wave form measured by MR imaging used to calculate the pulsatile velocity profile.

C, Velocity profile, $v(r,t)$, from the center of the vessel to the wall at 16 frames over the cardiac cycle. Each profile is the sum of harmonic components at one frame.

D, Wall shear rate over the cardiac cycle, and the slope of the velocity profile at the vessel wall.

to improve with more signal averaging. At one, two, and four acquisitions, the variance of measurements derived from LE* was approximately four times greater than that for LE or QE. The variance of LE* measurements, however, dropped dramatically at eight and 16 acquisitions to the range of the LE and QE variance. Post-hoc analysis indicated that none of the QE measurements were significantly different from one another. LE tended to consistently underestimate shear rate regardless of the number of acquisitions, whereas LE* and QE tended to more closely approximate the predicted value.

The results of the in vitro experiments, which used a physiological carotid flow waveform, are shown in Figure 3. Figure 3A is a plot of the average velocity waveform, $\bar{v}(t)$. Close correspondence was found between the average velocity measured with an ultrasonic flow probe and that measured with PC MR imaging. At each point of velocity measurement in the cardiac cycle, a near coincidence of the MR measurement and the flow waveform was synthesized from the inverse Fourier transform, because, for these points, the waveform is an exact solution. The decomposition of $\bar{v}(t)$, the average velocity over the vessel lumen measured by MR imaging, into a series of Fourier harmonics is shown in Figure 3B. Each harmonic results in a velocity profile, which when summed over all harmonics, results in the velocity profile, $v(r,t)$, for $\bar{v}(t)$ (Fig 3C). Shear rate can then be derived by calculating the spatial derivative of these profiles at the vessel wall (Fig 3D).

The results of shear rates obtained by using LE, LE*, and QE in the in vitro phantom pulsatile flow experiments as compared with those obtained with the ultrasonic flow probe are shown in Figure 4. Shear rates derived from the Womersley equation

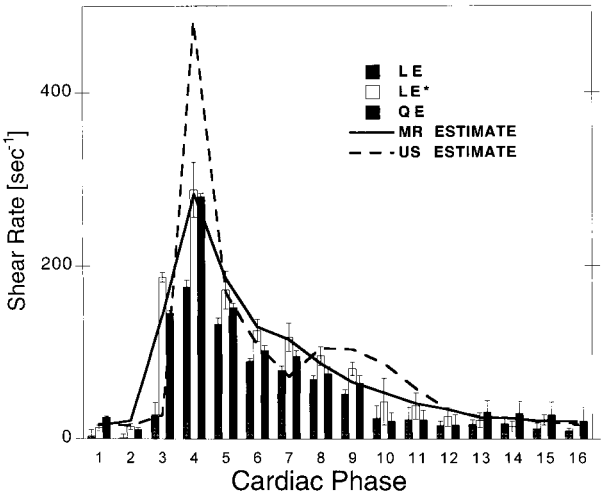

FIG 4. Measured shear rates for pulsatile flow experiment in the phantom. An ultrasonic flow probe provided an independent estimate of average velocity.

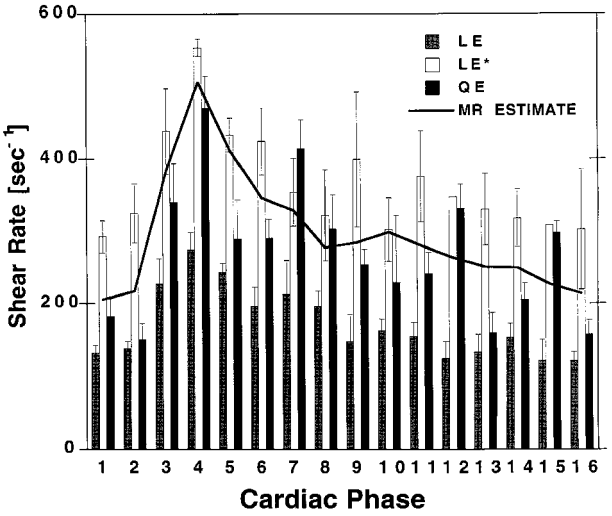

FIG 5. Measured shear rates obtained in a volunteer.

were calculated by using both the PC MR data and the ultrasonic flow probe estimates of $\bar{v}(t)$ and were found to have a reasonable correspondence. However, it is evident that the greatest error occurred during peak systole, reflecting the decreased accuracy of retrospectively gated PC MR imaging in measuring rapidly changing velocities (32). The root mean squared discrepancies between the LE, LE*, and QE results as compared with the shear rates calculated from the data in Equation 12 were 45.5 s^{-1}, 13.4 s^{-1}, and 16.9 s^{-1}, respectively. The maximum deviations were 115 s^{-1}, 44.4 s^{-1}, and 33.4 s^{-1}, respectively. An estimate of the accuracy of these measurements may be determined by expressing the root mean squared differences as a percentage of the time-averaged wall shear rate calculated from Equation 12. The quotients for LE, LE*, and QE were 59%, 17%, and 22%, respectively. Analysis of variance of the residual LE, LE*, and QE measurements determined a significant difference between LE and baseline ($P < .0001$), whereas LE* and QE did not differ significantly from baseline ($P = .89$ and $P = .13$, respectively). Mean residuals indicated that LE* most closely matched the baseline (mean residual = 0.95 s^{-1}, standard error [SE] = 3.4 s^{-1}), although QE did not differ significantly (mean residual = 10.5 s^{-1}, SE = 3.4 s^{-1}), and LE consistently underestimated shear rate (mean residual = −32.0 s^{-1}, SE = 13.8 s^{-1}).

In Vivo Results

Shear rate estimates obtained with the LE, LE*, and QE algorithms over the cardiac cycle in one volunteer are shown in Figure 5. The agreement between the data and the shear rates calculated from Equation 12 is fair, with root mean squared errors of 149 s^{-1}, 99.1 s^{-1}, and 97.6 s^{-1}, and maximum deviations of 372 s^{-1}, 151 s^{-1}, and 259 s^{-1}, respectively. As defined above, the percentages of errors for the three methods were 98.5%, 28.5%, and 36.1%, respectively. Scatter plots for all the volunteer data are presented in Figure 6. Statistical analysis of the residual data collected in five healthy volunteers revealed a statistically significant difference ($df = 3$, $F = 106$, $P < .0001$) for the main effect of the method (ie, the method of shear rate calculation from the same PC velocity data). The post-hoc analysis indicated that all three methods differed significantly ($P < .0001$), LE and LE* differed from baseline ($P < .0001$), and QE did not differ significantly from baseline ($P = .36$). The mean residuals for each method indicated that QE most closely matched the baseline (mean residual = −10.2 s^{-1}, SE = 10.9 s^{-1}). LE highly underestimated baseline (mean residual $^{-1}30$ s^{-1}, SE = 8.09 s^{-1}), and LE* overestimated baseline (mean residual = 66.7 s^{-1}, SE = 8.28 s^{-1}). Using the QE method, the average wall shear rate measurement over the entire cardiac cycle was 270 s^{-1} (SD = 114 s^{-1}), and the average peak systolic shear rate was 439 s^{-1} (SD = 135 s^{-1}). Assuming a whole-blood viscosity of 3 cP, these average values correspond to an average shear stress on the vessel wall of 8.10 dyne/cm^2 and a peak systolic wall shear stress of 13.2 dyne/cm^2.

Discussion

The dynamic forces that flowing blood exerts on the vasculature are important in the initiation and progression of atherosclerosis, the growth and rupture of saccular aneurysms, and the cerebral dysfunction and hemorrhage associated with arteriovenous malformations (1–4, 8–14). The ability to measure and to monitor these forces in a noninvasive manner would contribute significantly to our understanding of these conditions. Furthermore, such measurements could lead to a set of parameters used to stratify the risk that these lesions pose to individuals because of the forces acting on the living vascular wall (13). This study was undertaken as a step toward further development of a practical technology of the noninvasive measurement of

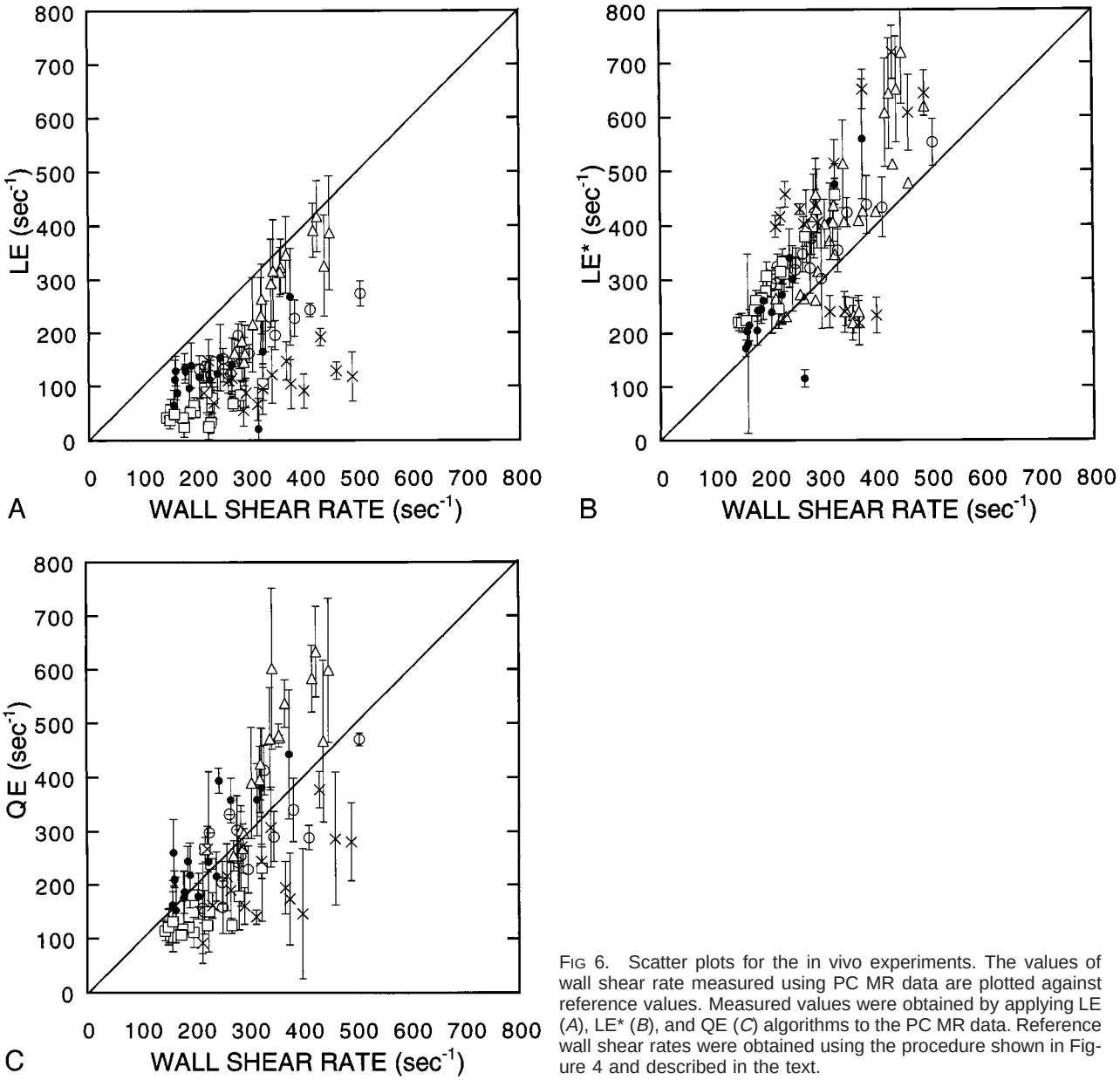

FIG 6. Scatter plots for the in vivo experiments. The values of wall shear rate measured using PC MR data are plotted against reference values. Measured values were obtained by applying LE (*A*), LE* (*B*), and QE (*C*) algorithms to the PC MR data. Reference wall shear rates were obtained using the procedure shown in Figure 4 and described in the text.

hemodynamic stress in clinically encountered cerebrovascular lesions. Findings of previous studies have established the relationships between the distribution and severity of carotid bifurcation atherosclerosis. Zarins et al compared the shear stress in steady flows within casts of autopsy specimens, revealing that early lesions occur principally in regions of flow separation, low wall shear stress, and departure from unidirectional flow (9). Ku et al reported that plaques tend to form in areas of low shear stress and that oscillations in the direction of wall shear stress may enhance atherogenesis (8). Both these studies used in vitro laser Doppler velocimetry. Doppler sonography has previously been used to study the hemodynamics of the carotid bifurcation (33). The aortic bifurcation has been extensively studied as a model of atherogenesis near arterial bifurcations and fusiform aneurysm formations (34, 35). Two previous studies have used MR imaging for the noninvasive measurement of wall shear stress within the living human aorta (19, 20). To our knowledge, this is the first report of the use of shear measurements derived from MR imaging velocity measurements to study carotid artery wall shear stress.

Lou et al point out that an instrument well suited for the measurement of shear stress should have a high spatial resolution close to the vessel wall and a high-frequency response for measuring shear rates in pulsatile flows (23). In addition, the instrument should not disturb the flow. Certainly, MR imaging meets the third criterion but only marginally fulfills the first two. Several simplifying conditions and assumptions were introduced into the experiment and analysis regarding geometry, viscosity, and vessel wall compliance. Measurements

were obtained in the straight portion of the cervical internal carotid artery to avoid the necessity of using more sophisticated finite-element computational algorithms to calculate the expected value of wall shear stress in the complex geometry of diseased arteries. The calculated shear values assume rigidity of the arterial wall, which in reality is viscoelastic. Although the deformable nature of the vessel may be important in pressure wave propagation, the effect on local velocity profile and wall shear stress is relatively small (35). Since the diameter of the carotid artery is large compared with the diameter of the red blood cell, the assumption of Newtonian viscosity should not introduce a large error in calculating velocity profiles and shear rates in comparison with in vivo measurements (35). In this study, we have addressed errors incurred in using a 2D PC technique and have investigated the errors involved in the analysis of the MR data using LE-, LE*-, and QE-processing algorithms. For these methods, the principal sources of systematic errors are the finite spatial and temporal resolutions of the MR imaging flow measurements. The finite spatial resolution leads to a nonlinear averaging of the velocity measurement across the pixel and also to uncertainty in locating the vessel wall relative to the image matrix (25). Both of these effects are important, because measurement of the shear rate depends on the ability to accurately and simultaneously observe the velocity of flowing blood near the wall as well as the position of the wall itself. Thus, to obtain an accurate approximation of the wall shear rate, a measurement of the velocity profile near the wall must be obtained or estimated with high accuracy. Each of the three methods used for calculating the wall shear rate attempts to overcome, to varying degrees, these sources of errors. LE is the simplest scheme. No correction for wall position is made, and it is assumed that a linear velocity profile exists near the wall. In comparison, when LE* is used, an attempt is made to correct for wall position within the appropriate pixel; however, it is still assumed that a linear velocity profile exists near the vessel wall. Calculations using the QE method assume that a parabolic velocity profile exists, thereby inherently estimating the wall position when $v = 0$. This method requires that velocity estimates be obtained at three positions, which may lead to spatial averaging. Limitations of finite temporal resolution also affect the accuracy of shear estimates. If retrospectively gated PC data are used, as it was in these experiments, then the measured MR flow waveform does not follow all the features of the true waveform (32) (Fig 4).

Random errors are introduced in calculations obtained with all techniques, simply because the underlying PC velocity data contain noise. For those pixels that contain only a small amount of flowing blood, only a small phase shift is produced, and this may then be obscured by noise. It thus becomes difficult to identify the pixel that contains both vessel lumen and vessel wall. In other words, because of the very slow flow immediately adjacent to a vessel wall, the small signal that this flow imparts to the PC velocity data, and the inherent noise in the PC technique, the pixel chosen as the one that contains both lumen and wall may actually lie within the vessel lumen. In addition, our consideration of relative wall and pixel is one dimensional, whereas, in reality, it is a two-dimensional problem; that is, measurements are obtained within square pixels superimposed onto a larger circular cross section.

The velocity-encoding value of 100 cm/s was chosen for our in vitro experiments on the basis of preliminary experience in acquiring in vivo data to avoid aliasing and because of the need to unwrap the phase-difference velocity measurements, which is cumbersome to achieve in practice. At the low flow rates chosen to remain well within the laminar range, the relatively high velocity-encoding value would tend to reduce the signal-to-noise ratio and thus increase the SD of our in vitro measurements. We attempted to minimize all errors by estimating shear rate at the four cardinal positions of the vessel.

The results of shear measurements for constant flow in a straight tube indicate that the accuracy of calculations obtained with the LE and QE techniques are insensitive to the number of acquisitions. Since calculations obtained with the LE* method are more sensitive to the noise effects discussed above, accuracy with this method tends to improve as the number of acquisitions increase. The velocity and wall shear calculations for pulsatile flow in the phantom experiments indicate a close, but imperfect, correspondence between those derived from the independent measurements (ultrasonic flow probe) and the data obtained by MR imaging.

In previous reports, LE has been shown to systematically underestimate wall shear stress (22, 23). LE* was shown to systematically overestimate wall shear stress in this study. The reason for this is not clear but is likely tied to the pixel size relative to the vessel diameter (5 to 10 mm in this study, vs $>$25 mm in previous studies [19, 20]). QE measurements were shown not to differ significantly from the predicted values, whereas the LE* measurements did, although the standard errors of the LE* and QE measurements were similar. This is because the LE* measurements tended to more consistently overestimate the predicted value, whereas the QE values varied more evenly above and below the predicted values.

Conclusion

Our results establish the feasibility of deriving fairly accurate wall shear rates in the carotid artery using PC MR data. The QE algorithm appears to be the most accurate of the three that were tested, although the variability of individual measurements using the LE* and QE methods is fairly high. Useful results were obtained in a single acquisition us-

ing QE. These results support further efforts to develop techniques for the noninvasive measurement and mathematical simulation of the hemodynamic forces of blood flow in cerebrovascular disease.

References

1. Caro CG, Fitz-Gerald JM, Schroter RC. **Atheroma and arterial wall shear: observation, correlation and proposal of a shear dependent mass transfer mechanism for atherogenesis.** *Proc R Soc Lond B [Biol]* 1971;177:109–159
2. Orel VE. **Mechanochemiemission and atherogenesis.** *Med Hypotheses* 1995;45:343–344
3. Fry DL. **Acute vascular endothelial changes associated with increased blood velocity gradients.** *Circ Res* 1968;22:165–197
4. Langille BL. **Blood flow-induced remodeling of the artery wall.** In: Bevan JA, Kaley G, Rubanyi GM, eds. Flow Dependent Regulation of Vascular Function. Clinical Physiology Series of the American Physiological Society. Oxford: Oxford University Press; 1995;13:277–297
5. Song SM, Leahy RM, Boyd DP, Brundage BH, Napel S. **Determining cardiac velocity fields and intraventricular pressure distribution from a sequence of ultrafast CT cardiac images.** *IEEE Trans Med Imaging* 1994;13:386–397
6. Adler RS, Chenevert TL, Fowlkes B, Pipe J, Rubin JM. **Calculation of pressure gradients from MR velocity data in a laminar flow model.** *J Comput Assist Tomogr* 1991;15:483–488
7. Bird RB, Stewart WE, Lightfoot EN. **Transport Phenomena.** New York: Wiley; 1960;71–122
8. Ku DN, Giddens DP, Zairns CZ, Glagov S. **Pulsatile flow and atherosclerosis in the human carotid bifurcation: positive correlation between plaque localization and low and oscillating shear stress.** *Arteriosclerosis* 1985;5:293–302
9. Zarins CK, Giddens DP, Bharadvaj BK, Sottiural VS, Mbon RJ, Glgov S. **Carotid bifurcation atherosclerosis: quantitative correlation of plaque localization with flow velocity profiles and wall shear stress.** *Circ Res* 1983;53:502–514
10. Friedman MH, Hutchins GM, Bargeron CB, Deters OJ, Mark FF. **Correlation between intimal thickness and fluid shear in human arteries.** *Atherosclerosis* 1981;39:425–436
11. Burleson AC, Strother CM, Turitto VT. **Computer modeling of intracranial saccular and lateral aneurysms for the study of their hemodynamics.** *Neurosurgery* 1995;37:774–782
12. Rossitti S, Svendsen P. **Shear stress in cerebral arteries supplying arteriovenous malformations.** *Acta Neurochir (Wien)* 1995; 137:138–145
13. Strother CM. **Understanding the natural history of cerebral aneurysms.** *AJNR Am J Neuroradiol* 1998;19:1183–1184
14. Hademos GJ, Massoud TF, Vinuela F. **A biomathematical model of intracranial arteriovenous malformations based on electrical network analysis: theory and hemodynamics.** *Neurosurgery* 1996;38:1005–1014
15. Moran PR. **A flow velocity zeugmatographic interlace for NMR imaging in humans.** *Magn Reson Imaging* 1982;1:197–203
16. Dumoulin CL, Souza SP, Walker MF, Wagle W. **Three dimensional phase contrast angiography.** *Magn Reson Imaging* 1989; 9:139–149
17. Moore JA, Steinman DA, Ethier CR. **Computational blood flow modelling: errors associated with reconstructing finite element models from magnetic resonance images.** *J Biomech* 1998;31: 179–184
18. Urchuk SN, Plewes DB. **MR measurement of pulsatile pressure gradients.** *J Magn Reson Imaging* 1994;4:829–836
19. Oshinski JN, Ku DN, Mukundan S, Loth F, Pettigrew RI. **Determination of wall shear stress in the aorta using MR phase velocity mapping.** *J Magn Reson Imaging* 1995;5:640–647
20. Oyre S, Pedersen EM, Ringgaard S, Boesiger,Paaske WP. **In vivo wall shear stress measured by magnetic resonance velocity mapping in the human abdominal aorta.** *Eur J Vasc Endovasc Surg* 1997;13:263–271
21. Frayne R, Rutt BK. **Measurement of fluid-shear rate by Fourier-encoded velocity imaging.** *Magn Reson Med* 1995;34: 378–387
22. Steinman DA, Smith RF, Ethier CR, Rutt BK. **Wall shear stress via MR: linear or quadratic extrapolation?** In: Proceedings of the Society for Magnetic Resonance, Nice, France, 1995: 322
23. Lou Z, Yang WJ, Stein PD. **Errors in the estimation of arterial wall shear rates that result from curve fitting of velocity profiles.** *J Biomech* 1993;26:383–390
24. Polzin JA, Korosec FR, Wedding KL, et al. **Effect of through-plane myocardial motion on phase-difference and complex difference measurements of absolute coronary artery flow.** *J Magn Reson Imaging* 1996;6:113–123
25. Hamilton CA. **Correction of partial volume inaccuracies in quantitative phase contrast MR angiography.** *Magn Reson Imaging* 1994;12:1127–1130
26. Rickey DW, Picot PA, Christopher DA, Fenster A. **A wall-less vessel phantom for Doppler ultrasound studies.** *Ultrasound Med Biol* 1995;21:1163–1176
27. Frayne R, Holdsworth DW, Gowman LM, et al. **A computer-controlled flow simulator for MR flow experiments.** *J Magn Reson Imaging* 1992;2:605–612
28. Frayne R, Steinman DA, Ethier CR, Rutt BK. **Accuracy of MR phase contrast velocity measurements for unsteady flow.** *J Magn Reson Imaging* 1995;5:428–431
29. Milnor WR. **Hemodynamic.** 2nd ed. Baltimore: Williams & Wilkins; 1982;347–348
30. Nichols WW, O'Rourke MF. **McDonald's Blood Flow in Arteries.** Philadelphia: Lea & Febiger; 1990;36–38
31. Keppel G. **Design and Analysis.** Englewood Cliffs, NJ: Prentice Hall; 1982;157–159
32. Frayne R, Rutt BK. **Frequency response of retrospectively gated phase contrast MRI: effect of interpolation.** *J Magn Reson Imaging* 1993;3:908–917
33. Ku DN, Phillips DJ, Giddens DP, Strandness DE. **Hemodynamics of the normal human carotid bifurcation: in vitro and in vivo studies.** *Ultrasound Med Biol* 1985;11:13–26
34. Duncan DD, Bargeron CB, Borchardt SE, et al. **The effect of compliance on wall shear in casts of a human aortic bifurcation.** *J Biomech Eng* 1990;112:183–188
35. Friedman MH, Bargeron CB, Duncan DD, Hutchins GM, Mark FF. **Effects of arterial compliance and non-Newtonian rheology on correlations between intimal thickness and wall shear.** *J Biomech Eng* 1992;114:317–320